An Optimal Control Approach for Ultrasound Induced Heating

Matti Malinen, Tomi Huttunen, Jari P. Kaipio*

May 20, 2003

*Authors are with the Department of Applied Physics, University of Kuopio, P.O. Box 1627, 70211 Kuopio, Finland (E-mail: Jari.Kaipio@uku.fi, Matti.Malinen@uku.fi, Tomi.Huttunen@uku.fi).

Abstract

The absorbed energy of ultrasound and microwaves is changed into heat in a dissipative medium. This wave field induced heating has numerous applications in industry and medicine. In these applications the ability to control the resulting heat distribution is essential. In this paper we design a controller for quadratic cost criteria in the ultrasound induced heating problem in inhomogeneous media. In this approach the time-harmonic pressure fields are computed from individual wave sources by solving the Helmholtz equation with the ultra weak variational formulation. The equations that define the controller are derived from the Hamiltonian form of the system, which results in a large dimension nonlinear control problem. As an example we study a numerical simulation that resembles an ultrasound therapy problem in 2D. The simulation shows that feasible solutions can be obtained with this approach.

Key words: Ultrasound, Heating, Nonlinear control, Ultra weak variational formulation.

1 Introduction

When ultrasound, laser or microwaves are absorbed in a dissipative medium, the absorbed energy is turned into heat. This wave field induced heating has numerous applications in medicine and industry. These applications result in control problems of how the desired temperature distribution or absorbed thermal dose can be achieved.

The industrial applications of the wave field induced heating are often related to material science and sonochemistry. In material science plastics and metals can

be welded together by using the absorbed heat of the ultrasound or microwave field (Mason 2000), (Ku *et al.* 2001), (Zohm *et al.* 2000). In sonochemistry, the heating effect of the ultrasound is used as a catalyst to chemical reactions (Mason 2000). The temperature distribution optimization in wave field induced heating problems in medical applications is usually done by optimizing the specific absorption rate (SAR) (Bardati *et al.* 1995), (Köhler *et al.* 2000). Steady-state optimization methods have also been used in this type of problems (Nikita *et al.* 1993), (Lin *et al.* 1992).

The medical applications include hyperthermia treatment and ultrasound surgery. In hyperthermia treatment the effect of the radiotherapy is improved by heating the cancerous tissue to 43-45 °C for over 30 minutes (Lagendijk 2000), (Diederich and Hynynen 1999), (ter Haar 1999). In ultrasound surgery the cancerous tissue can be destroyed by rising the temperature to cytotoxic level (Chapeleon *et al.* 1999), (Visioli *et al.* 1999). The desired temperature in tumor can be up to 70 °C (Crum and Hynynen 1996). Although lower temperatures could also be used, the use of high temperatures can reduce the treatment time significantly (Hynynen 1996). Focused ultrasound and microwaves are used to induce a distributed heat source in these treatments.

The PID type controllers with pre-focused ultrasound fields are used to control the temperature trajectories (VanBaren and Ebbini 1995), (Johnson *et al.* 1990), Lin *et al.* 1990), (Doss 1985) as well as the inverse dynamics approach (Mattingly *et al.* 2000) and fuzzy logic controllers (Chen *et al.* 1999). In these controllers the main point is to obtain the desired temperature distribution with pre-focused ultrasound fields. The scanning path of the focus is pre-calculated in these controllers and they alter only the applied power i.e. the amplitude, not the phase of

the ultrasound waves. These approximations result in linear controller structures, which is implementationally convenient but is usually clearly inferior in performance when compared to more rigidly derived controllers. Steady-state optimization has been used also used to determine the optimal driving parameters for electromagnetic phased array system in (Kowalski and Jin 2000). In the study made in (Kowalski and Jin 2000) the phase and amplitude of the transducers were computed directly from the nonlinear optimization problem.

In this paper we propose an approach in which the ultrasound field is controlled by adjusting the amplitudes and the phases of each transducer individually. The absorbed energy of the ultrasound waves results in a distributed quadratic source term in the heat equation. The controller proposed here is of the feedforward (FF) type and it is not based on feedback during the sonication. Furthermore, this control method is not based on pre-computed focused fields. The main difference in this paper and (Kowalski and Jin 2000) is that our controller optimizes the transient trajectory while (Kowalski and Jin 2000) discusses only the maintaining of the steady state. This is a major difference when certain end applications such as ultrasound surgery are considered in which the main contribution of the thermal dose is due to the transient. Furthermore, the proposed method takes into account also the transducer limitations.

As the first step, the time-harmonic solution of the generally inhomogeneous Helmholtz problem is solved for each source individually. The solutions are computed with the recently proposed full wave method, the ultra weak variational formulation (UWVF). Standard finite element methods can usually not be used to compute the wave field at ultrasonic frequencies due to required high element-per-wavelength ratio.

The resulting control problem is nonlinear and is – in spite of the use of the UWVF – still large dimensional. However, the overall dimension of the problem is only a fraction of what it would be with standard FE methods.

The performance criterion of the approach is basically a quadratic cost that is related to the temperature distribution and control variable evolution smoothness. However, there are two complications. First, in practical applications the powers of the individual transducers are limited. Second, the mapping from relevant control variables to the temperature evolution is nonlinear. Thus the problem is turned into the minimization of a more general nonlinear cost function with nonlinear inequality constraints.

The rest of the paper is organized as follows. In Section II we review the ultra weak variational formulation for the Helmholtz problem and the FEM solution of the bioheat equation. In Section III we formulate the control problem and derive the solution. In Section IV we present a nontrivial simulation. In the simulation we consider an example that resembles ultrasound therapy problem in which the aim is to heat biological tissue. The simulation is carried out in 2D and does therefore not correspond to a realistic ultrasound therapy situation. We point out that the contribution of the paper is not ultrasound therapy but rather a new distributed parameter control approach for the heating of inhomogeneous material with ultrasound. Section V is dedicated to the results from the simulations and Section VI is the discussion of the features of the method. Section VII is dedicated to conclusions and extensions of the proposed approach.

2 Physical models and computational approximations

2.1 Helmholtz problem

Linear acoustic wave propagation and scattering in quiescent heterogeneous media is characterized by the wave equation

$$\nabla \cdot \left(\frac{1}{\rho}\nabla P\right) - \frac{1}{\rho c^2}\frac{\partial^2 P}{\partial t^2} = 0 \tag{1}$$

where P is acoustic pressure, ρ is density and c is the speed of sound. In the time-harmonic case we have $P(r,t) = p(r)e^{i\omega t}$, where $r = r(x,y)$ is the spatial variable, and the space dependent part of the pressure field is the solution of the inhomogeneous Helmholtz equation

$$\nabla \cdot \left(\frac{1}{\rho}\nabla p\right) + \frac{\kappa^2}{\rho}p = 0, \tag{2}$$

with wave number κ. In dissipative media the wave number is of the form $\kappa = 2\pi f/c + i\alpha$ where f is the frequency of the wave field and α is the absorption coefficient (Bhatia 1967).

Together with suitable boundary conditions the Helmholtz problem (2) can be solved using a variety of techniques. The standard tools have been the finite difference methods (FD) and the finite element methods (FEM) (Ihlenburg 1998). A common feature of these methods is the requirement of certain number of discretization points or elements per wavelength – usually 10 to 15. For high wave numbers this requirement results in very large problems with often intolerable computational burden. To avoid this problem ray approximations have been used to compute pressure fields with ultrasound frequencies, see e.g. (Fan and Hynynen 1992), (Kühnicke

1996), (Botros *et al.* 1997) and (Botros *et al.* 1998). However, this approach becomes increasingly complicated in complex geometries including multiple material interfaces and in practice impossible in the case of spatially continuously varying material parameters.

An alternative approach is to use novel full wave methods which allow the incorporation of a priori information of the solutions to the approximation subspaces. These methods include the partition of unity methods (PUM) (Babuska and Melenk 1997), the least squares methods (Monk and Wang 1999), and the ultra weak variational formulation (UWVF) (Cessenat and Despres 1998). Compared with the standard finite elements these methods can reduce the computational burden significantly. In this paper we use the UWVF to solve the acoustic wave field. The method is outlined in the Appendix. The advantage of the UWVF is – in addition to the reduced number of unknowns – that it is possible to adjust the distribution of unknowns

2.2 Bioheat equation

In biological tissues the temperature evolution is usually approximated with the so-called bioheat equation (Pennes 1948)

$$\rho C_{\mathrm{T}} \frac{\partial T}{\partial t} = \nabla \cdot k \nabla T - w_{\mathrm{B}} C_{\mathrm{B}} (T - T_{\mathrm{A}}) + Q, \tag{3}$$

where T is the temperature, ρ is the density of the medium, C_{T} is the heat capacity of tissue, w_{B} is the perfusion due to blood flow, C_{B} is the heat capacity of blood and T_{A} is the arterial blood temperature and Q is the distributed heat source. Furthermore, the heat source term for the time-harmonic acoustic pressure is (Pierce 1991)

$$Q = \frac{\alpha |p|^2}{\rho c}. \tag{4}$$

In this paper we use the Helmholtz equation for the wave field computing and thus neglect the nonlinear effects in wave propagation. This is a commonly made simplification, since the nonlinear effects are very small with pressure amplitudes that are considered here. When nonlinear effects are neglected the total field is the sum over the individual fields. With m separate transducers the total field is $p = \sum_{k=1}^{m} p_k$. In many applications it is natural to consider cases in which several transducers are used. For example in the medical applications the number of the transducers varies from 16 to 512 (Daum and Hynynen 1999), (Clement *et al.* 2000).

In the time-harmonic case the temporal and spatial dependence of the wave fields p_k can be separated and we can write

$$p_k = \tilde{u}_k(t)\widetilde{C}_k(r)e^{i\omega t} \ , \tag{5}$$

where $\tilde{u}_k(t) \in \mathbb{C}$ determine the amplitude and phase of the transducer source so that $\widetilde{C}_k(r)$ are the time-harmonic solutions of the Helmholtz problems with single point sources of unit source strengths. The main difference between the common steady state focusing (Ebbini and Cain 1989), (Botros *et al.* 1997) and the control method presented here is that the control variable $\tilde{u}_k(t)$ is also the function of time. The total heat source can be written as

$$Q(r,t) = \frac{\alpha(r)}{\rho(r)c(r)}\,|p|^2 = \frac{\alpha(r)}{\rho(r)c(r)}\left|\sum_{k=1}^{m}\tilde{u}_k(t)\widetilde{C}_k(r)\right|^2 \ . \tag{6}$$

The bioheat equation is discretized according to the usual semidiscrete scheme in which the spatial variable is handled with the Galerkin scheme and the resulting system of ordinary differential equations with appropriate (implicit) schemes such as backward Euler or Runge-Kutta (Johnson 1987). We employ the implicit Euler scheme in this paper. The only term that requires some explanation is the discretization of Q, which can be found in Appendix B.

We define the control variables $u_k = \mathrm{Re}\,\tilde{u}_k,\ k = 1, \ldots, m$ and $u_{k+m} = \mathrm{Im}\,\tilde{u}_k,\ k = 1, \ldots, m$ and the corresponding vector $u \in \mathbb{R}^{2m}$. Define also $\widehat{C}_k = (\widetilde{C}_k(r_1), \ldots, \widetilde{C}_k(r_N))^{\mathrm{T}}$ and $\widehat{C} = (\widehat{C}_1, \ldots, \widehat{C}_m) \in \mathbb{R}^{N \times m}$. We can then write the source term in the form

$$Q_{\mathrm{D}}(t) = \widetilde{M}[I, I]\big(Bu(t)\big)^2 = \widetilde{M}_{\mathrm{D}}\big(Bu(t)\big)^2 \,, \tag{7}$$

where $I \in \mathbb{R}^{N \times N}$ is the identity matrix, $\widetilde{M}$ is a modified mass matrix (for details, see Appendix B), $(\cdot)^2$ refers here to element wise squares and

$$B = \begin{pmatrix} \mathrm{Re}\,\widehat{C} & -\mathrm{Im}\,\widehat{C} \\ \mathrm{Im}\,\widehat{C} & \mathrm{Re}\,\widehat{C} \end{pmatrix} \tag{8}$$

The major difference between the proposed control method and earlier work on the temperature control of the ultrasound induced heating lies in Eq.(7). In the proposed approach we are bound to solve the optimal phase and amplitude trajectories directly rather than use the pre-focused ultrasound fields with pre-determined scanning paths. If ultrasound fields are pre-focused Eq.(7) reduces to the linear form, and the only control variable is the applied power to the transducers. However, this is not necessarily the optimal way to control the temperature distribution. Also, by separating the real and imaginary parts in Eq.(7) we can reduce the computational task of the proposed method. However, it is clear that the space of feasible solutions for the problem specified above contains also solutions that are of the type of scanning foci. The semidiscrete FEM approximation for the bioheat equation is then of the form

$$M\dot{T} = (G - w_{\mathrm{B}}C_{\mathrm{B}}I)T + w_{\mathrm{B}}C_{\mathrm{B}}MT_{\mathrm{A}} + \widetilde{M}_{\mathrm{D}}\big(Bu(t)\big)^2 \,, \tag{9}$$

where M is the (ordinary) mass matrix, G is the stiffness matrix and $\dot{T} = dT/dt$. In the following this is considered in the form

$$\dot{T} = AT + P + M_{\mathrm{D}}\big(Bu(t)\big)^2 \tag{10}$$

where we have made the obvious assignments. In the sequel we drop the time variable whenever there is no possibility of misunderstanding.

3 The implementation of the control method

3.1 The continuous time controller equations

Define the quadratic cost function

$$\tilde{J}(u,T;t) = \frac{1}{2}\int_0^{t_f} \left\{ \|T(t) - T_{\rm d}(t)\|_\vartheta^2 + \sum_{k=1}^{2m} s_k \left(\frac{du_k(t)}{dt} \right)^2 \right\} dt \ , \tag{11}$$

where $T_{\rm d} = T_{\rm d}(r,t)$ is the desired temperature distribution and s_k are weights for the time derivative of the input thus enforcing smoothness of the control variables. Further, $\|T(t) - T_d(t)\|_\vartheta^2 = \int_\Omega \vartheta(r)\big(T(r,t) - T_{\rm d}(r,t)\big)^2\, dr$.

In practice the maximum power or pressure amplitude is constrained so that the relevant control problem is of the form

$$\min_u \tilde{J}(u,T;t) \qquad \text{subject to } u_k^2 + u_{k+m}^2 \le \zeta \quad \text{for all } k = 1,\ldots,m \tag{12}$$

where we can take $\zeta = 1$ with an appropriate change of variables. This is a quadratic problem with quadratic inequality constraints. Due to the nonlinear constraints and the nonlinearity of the mapping $u \mapsto T$ we have to resort to numerical minimization methods. Furthermore, we approximate the inequality constraint by introducing an additional nonlinear penalty so that the we can define the cost function that is adopted in this paper as

$$J(u,T) = \tilde{J}(u,T) + \chi_R(u) \tag{13}$$

where $R \in \mathbb{R}$ and

$$\chi_R(u) = \frac{1}{2}\int_0^{t_f} \sum_{k=1}^{2m} R^{-1} \exp\big(2R|u_k|\big)\, dt \tag{14}$$

With all other factors fixed, the parameter R is relatively easy to adjust so that the constraint (12) is fulfilled with adequate accuracy.

Denote $du_k(t)/dt = \dot{u}_k(t)$. The Hamiltonian of the control problem is now (Stengel 1994)

$$\begin{aligned} H(u, \dot{u}, T, \dot{T}) &= \frac{1}{2}\left\{ \|T - T_{\mathrm{d}}\|_{\vartheta}^2 + \sum_{k=1}^{2m} s_k \dot{u}_k^2 + \sum_{k=1}^{2m} R^{-1} \exp\left(2R|u_k|\right) \right\} \\ &\quad + \lambda^{\mathrm{T}}\left(AT + P + M_{\mathrm{D}}(Bu)^2 - \dot{T}\right) \end{aligned} \tag{15}$$

where $\lambda = \lambda(t) \in \mathbb{R}^N$, $t \in [0, t_f]$, is the Lagrange undetermined coefficient.

3.2 Solution of the optimal control with direct temporal discretization

The straightforward approach for the solution of the optimal control problem is to write down the Euler-Lagrange equations for the Hamiltonian, which results in a coupled system of (systems of) nonlinear differential equations. However, this approach leads to a very large dimensional nonlinear boundary value problem. The straightforward realization of the numerical solution for this system is notoriously problematic due to the instability of the subsystem describing the evolution of the Lagrange multiplier.

In this paper we solve the problem by directly discretizing the control and state variables as well as the Lagrange multiplier with respect to time and using a steepest descent type algorithm for computing the control variable. In the minimization procedure we employ a three-step approach, which involves the discretized derivatives of the complete Hamiltonian.

This three-step approach is an iterative nonlinear adaptation of the corresponding approach for linear systems and quadratic cost functions (Burl 1999), (Stengel

1994). In this approach with each iteration the state variable is first solved from the bioheat equation. Then the Lagrange multiplier can be calculated from the time-reversed co-state equation and finally the optimal control is solved from the stationary condition.

Let the temporal discretization constant for u be Δt and $N_T = t_f/\Delta t + 1$. In the sequel we denote the temporally discretized variables as $u_t = u(t\tau/\Delta t) \in \mathbb{R}^{2m}$, $\tau \in [0, t_f]$, $t \in [0, \ldots, N_T]$, with other variables denoted correspondingly. The discretized Hamiltonian is then of the form

$$\begin{aligned} H(u_t, T_t, \dot{T}_t) &= \frac{1}{2}\left(\|T_t - T_{\mathrm{d},t}\|_\vartheta^2 + \sum_{k=1}^{2m} s_k \left(u_{k,t} - u_{k,t-1}\right)^2 \sum_{k=1}^{2m} R^{-1} \exp\left(2|R|u_{k,t}\right) \right) \\ &\quad + \lambda^{\mathrm{T}} \left(AT_t + P + M_{\mathrm{D}}(Bu_t)^2 - \dot{T}_t \right) \ , \end{aligned} \tag{16}$$

where Δt^{-2} has been absorbed in s_k. We have for the co-state (Stengel 1994)

$$-\frac{\partial \lambda}{\partial t} = \frac{\partial H}{\partial T_t} = \vartheta \left(T_t - T_{\mathrm{d},t}\right) + A^{\mathrm{T}} \lambda_t \tag{17}$$

and for the stationary condition

$$\frac{\partial H}{\partial u_t} = H_{u_t} = L(u_t) + \lambda_t^{\mathrm{T}} F(u_t) \tag{18}$$

$$L(u_t) = \mathrm{sign}\left(u_t\right) \odot \exp(2R|u_t|) + S\left(u_t - u_{t-1}\right) \tag{19}$$

$$F(u_t) = 2M_{\mathrm{D}}\left(B \odot (Bu, \ldots, Bu)\right) \tag{20}$$

where $S = \mathrm{diag}\left(s_1, \ldots, s_{2m}\right)$, and $\odot$ denotes the element wise product of two matrices or vectors.

The time evolution for the bioheat and co-state equations is approximated with the implicit (backward) Euler approach so that we can write

$$T_{t+1} = (I - \Delta t A)^{-1} T_t + \Delta t (I - \Delta t A)^{-1} \left(P - M_{\mathrm{D}}(Bu)^2\right) \tag{21}$$

$$\lambda_{t-1} = (I - \Delta t A^{\mathrm{T}})^{-1} \lambda_t + \Delta t (I - \Delta t A^{\mathrm{T}})^{-1} \vartheta \left(T_t - T_{\mathrm{d},t}\right) \tag{22}$$

The stationary condition is pursued by the Levenberg-Marquardt type stabilized iteration with the search direction

$$H_{u_t} = \left(F(u_t)^{\mathrm{T}} F(u_t) + \mu I\right)^{-1} \left(L(u_t) + F(u_t)^{\mathrm{T}} \lambda_t\right) \ . \tag{23}$$

where μ is the stabilization parameter. In the iteration, the next control variable is computed as

$$u_t^{(\ell+1)} = u_t^{(\ell)} - \epsilon H_{u_t}^{(\ell)} , \tag{24}$$

where ϵ is the iteration step parameter and ℓ is the iteration round.

4 Simulations

4.1 Verification of the accuracy of the UWVF solver

The simulations were carried out in a 2D domain. The computational domain for simulations is shown in Figure 1. The domain consists of the three subdomains Ω_{I}, Ω_{II} and Ω_{III} with different physical parameters. The physical parameters are given in Table 1. There were 40 point sources located in a circle with radius of 4 cm around the computing domain. Between the point sources and subdomain Ω_{I} are assumed to be media with the same acoustic parameters as in Ω_{I}. in The geometry was chosen in order to assess the spatial accuracy of the controller. The domain was divided into 840 triangular elements and 445 vertex nodes. The maximum spacing between the nodes in this mesh was 4 mm. The ultrasound fields with frequency of 500 kHz were computed with the UWVF for each point source separately. In this example we consider a system and a specific application in which the maximum pressure amplitude is constrained to less than 1 MPa.

To stabilize the UWVF problem we chose the number of bases in the element Ω_j so that the L_1-condition number of the corresponding matrix block D_k was below a

predetermined value. We used the highest number of bases which gives the condition number below 10^8. See (Huttunen *et al.* 2002) for details of the adaptive scheme for the UWVF.

The accuracy of the UWVF solution was verified by setting the acoustic parameters of the domain Ω_{II} equal to the outermost domain Ω_{I} so that $c = 1500$ m/s, $\rho = 1000$ kg/m^3 and $\alpha = 0$ Nep/m. The material parameters in the domain Ω_{III} were the same than in Table 1. In this geometry the problem (26)-(28) reduces to a simple transmission problem through a circle for which a very accurate approximation can be computed with truncated Fourier series (Morse and Ingard 1968). This approximation was compared to the UWVF approximation.

The UWVF approximation was computed in the mesh of Figure 2. The number of bases N_j varied between 11 and 23. The relative discrete L_2 error of the UWVF solution for the transmission problem through the circle was 6.8 % which is a tolerable accuracy for test purposes.

Figure 2 represents the mesh and the normed intensity of the UWVF solution of the Helmholtz equation from point source 16. The maximum of the pressure field was 1 MPa for all wave fields. The scattering due to the strong acoustic mismatch between different material in the domains Ω_{II} and Ω_{III} is clearly seen in Figure 2. With the correct material parameters, the matrices C and B are constructed from these pre-computed fields.

4.2 The optimal control problem

The thermal properties of the subdomains were set to be equal. The thermal parameters used in simulations are given in Table II and they are similar to those in biological tissues (Skinner *et al.* 1998),Lin *et al.* 1990), (VanBaren and Ebbini

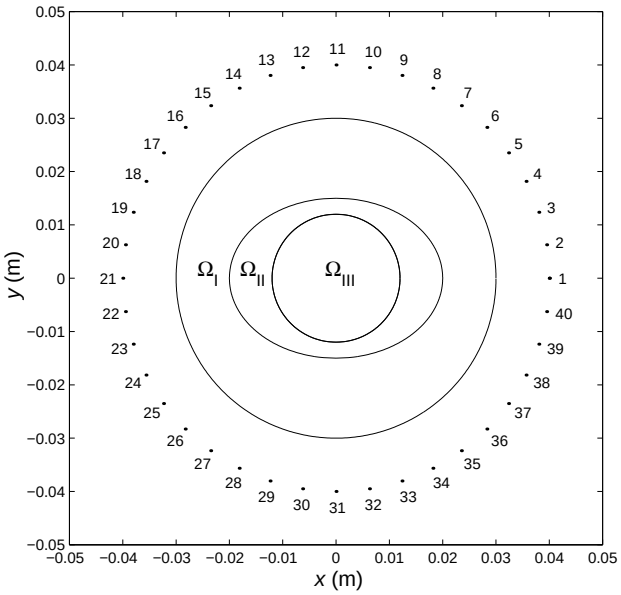

Figure 1: The computing domain. There are 40 point sources located around the computing domain (numbered $1, \ldots, 40$). Acoustic parameters are given in Table 1.

1995). The bioheat equation was computed by the semi-discrete FEM and the implicit Euler iteration.The time interval $t = [0, 10]$ s was discretized with Δt =0.1 s. The computing of the bioheat equation was accomplished in the same mesh as in which the Helmholtz equation. This can be done if the mesh is adequately dense also for the heat equation in which case we avoid interpolation between the two meshes. In any case the interpolation would be straightforward.

The optimal control u_t was computed with the algorithm given in Section 3. The target heat distribution was of the form of the letter "T" in the middle of Ω_{III}. The desired temperature in the target region was 45°C while the desired temperature in other parts of the computing domain was 37°C. The design criteria for the heating problem was to minimize heating in the strongly absorbing medium Ω_{II} as much as possible, while greater temperatures were allowed in the Ω_{III}. These requirements

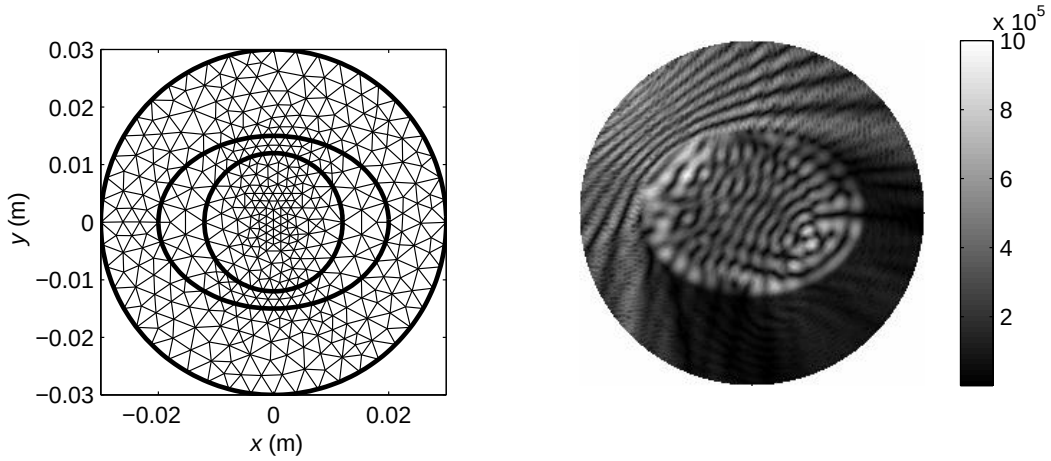

Figure 2: Left: The computing mesh that consists of the 840 elements and 445 nodes. Right: The normed $|p|$ distribution from the UWVF solution of the Helmholtz equation from point source 16.

Table 1: The Acoustic Parameters in Different Media for the Control Simulations.

Parameter	Ω_{I}	Ω_{II}	Ω_{III}
Speed of the sound c (m/s)	1500	2500	2000
Density ρ (kg/m^3)	1000	2000	1500
Absorption coefficient α (Nep/m)	0	4	2

Table 2: The Thermal Parameters for Control Simulations.

Heat capacity of the tissue C_t (J/kgK)	3700
Thermal conductivity of the tissue k_t (W/mK)	0.6
Perfusion by the blood flow w_b (kg/m^{3}s)	1
Heat capacity of the blood C_b (J/kgK)	3800
Arterial blood temperature T_a (°C)	37

to the heat distribution result in a difficult control problem, since Ω_{II} has twice greater absorption coefficient than the target domain and the spatial dimensions of the target are small. This type of control problems can be found for example in ultrasound surgery and hyperthermia treatment in which undesired heating must be minimized in a healthy tissue. In addition, in the case of ultrasound surgery of brain tumors, the subdomain which is to be heated, is located inside the skull, which absorbs ultrasound more than the brain tissue.

The weighting matrix ϑ for the temperature distribution was set to be diagonal with direct weighting for the temperature errors in each node point. The selection of weights for nodes depends on the relative costs based on medical consideration, for example the harm done by overheating nearby healthy tissue relative to not killing the tumor completely. Even then, as in all this type of controllers the weights have to be adjusted to the current problem more or less manually since there is no known systematic procedure (Burl 1999), (Stengel 1994). In this example we chose (based on nonmedical ad hoc considerations) for the nodes in Ω_{II} , Ω_{III} and the target "T" the weights 480, 300 and 400, respectively.

The design criteria for the input was to keep the maximum pressure below 1 MPa and to smooth the input trajectories. The weight for the controls was $R = 8$ and for the time derivative $s_k = 100$ for all k.

The Levenberg-Marquardt stabilization parameter was set to $\mu = 5000$. This choice corresponded to $\mu = 0.05\|F(u_t^{(0)})^T F(u_t^{(0)})\|_2$ which is often used in the Levenberg-Marquardt iteration. The iteration step parameter was chosen as $\epsilon = 0.009$. This ϵ was chosen to ensure the convergence. A more efficient approach would be to use line search and thus an iteration dependent step parameter. The inherent non-uniqueness of the phase was solved by setting the phase of the first

source to zero. The initial guess for the iteration was $u_{k,t}^{(0)} = 0.01$ for all k and t. As the iteration stopping criterion we used

$$\frac{J^{(\ell)} - J^{(\ell-1)}}{J^{(\ell)}} \leq 10^{-5} \tag{25}$$

where $J^{(\ell)}$ is the cost at iteration ℓ. With these parameters the controller iteration took 400-1000 rounds to satisfy the stopping criterion.

The spatial discretization has a great effect in this type of the controllers because the weighting of the temperature distribution is proportional to the discretization. If the computing mesh is too sparse, the results may not correspond to the actual physical problem Also, in order to avoid this so-called inverse crime we verify the computed results in another mesh than the one in which the control was carried out. This mesh is shown in Figure 3 and it consists of 1212 elements and 639 nodes. In this mesh, the maximum spacing between the nodes was 3 mm.

In this case the change to a more dense mesh did not have a significant effect i.e the temperature distribution did not change in this substitution. This indicates that the mesh was dense enough.

However, this discrepancy was clearly significant for meshes with less that 70% of the elements used here. Thus caution has to be exercised and multiple cross-checking should be carried out.

5 Results

The target and the controlled temperature distribution at the final time $t_f = 10$ s are shown in Figure 4. The desired temperature in the target is obtained fairly well. The controlled temperature distribution can be analyzed with several quality parameters which are discussed in (Köhler *et al.* 2000). We denote by T_{90} the

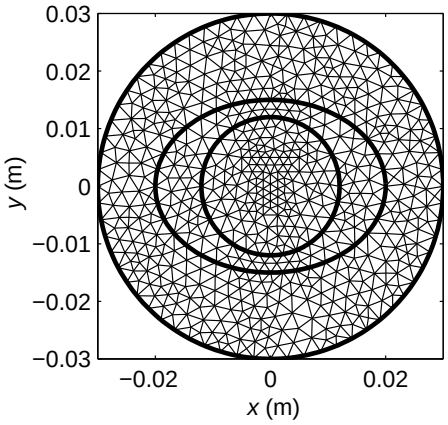

Figure 3: The mesh in which results were verified. The mesh consists of 1212 elements and 639 nodes.

temperature which is achieved in least 90 % of the target region. Furthermore, T_{ave} denotes the average temperature in the subdomains and the target, $T_{\max}$ is the maximum temperature reached in the subdomains and D_{42} is the percentage of the target in which the therapeutically relevant temperature 42 °C is reached. These criteria for the simulation are given in Table 3.

The average temperature in the target is lower than the desired temperature (= 45°C). The therapeutically relevant temperature D_{42} is achieved almost everywhere in the target region. The other topic in desired temperature distribution was to minimize the heating in Ω_{II}. As one can see from Table 3, the aim is reasonably well achieved. The average temperature in Ω_{II} is quite low and even the maximum temperature is lower than 42°C. The domain outside the target region, Ω_{III}, was heated much more than Ω_{II}. In addition to direct heating by adsorption, thermal diffusion transfers heat from the target into this region. However, the average temperature in this region is low, so that the major part of the Ω_{III} did not warm considerably.

Table 3: Quality criteria for the simulation.

Domain	$T_{\max}(^\circ\mathrm{C})$	$T_{\mathrm{ave}}(^\circ\mathrm{C})$	$D_{42}(\%)$	$T_{90}(^\circ\mathrm{C})$
Target	46.70	43.41	91.18	42.03
Ω_{II}	41.63	38.54	-	-
Ω_{III}	43.87	39.22	-	-

Figure 5 shows the maximum temperatures in absorbing subdomains and the nodes where the highest temperatures was. From Figure 5 can be seen that the maximum temperature was in the middle of the target when the minimum temperature in target was in the left side of the vertical part. The maximum temperature in subdomain Ω_{III} increases during the sonication. This is due to the diffusion.

The other design criteria concerned the control parameters. The corresponding phases and amplitudes for the sources 6, 16, 26 and 36 are shown in Figure 6. As one can see, the constraint of the amplitude $p \leq 1$ MPa is almost satisfied. The maximum amplitude of the sources was 1.04 MPa. The other cost to the sources was the weighting of the time derivative of the control variable u. This smoothes the phase and the amplitude of the input as a function of time. There are no abrupt changes in the phases and amplitudes, which shows that this criterion is also well satisfied.

The temperature evolution and the square root of the induced heat during the sonication are shown in Figures 7 and 8. During the last 3 s of sonication, there are no major changes in temperature distribution and the absorbed heat rate almost vanishes. This indicates also that controller would be able to maintain the obtained state also for longer time intervals.

Figures 7 and 8 show what is the advantage of the transient control as compared

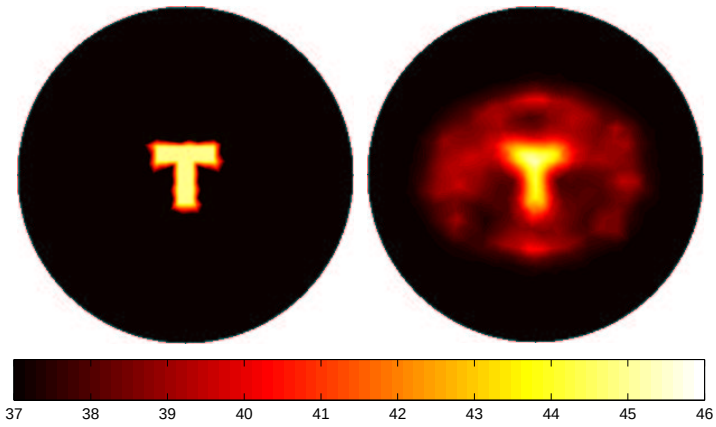

Figure 4: Left: The target temperature distribution with form of the letter T. The desired temperature in target is 45°C. Right: The controlled temperature distribution at the final time t_f =10 s.

to the steady-state optimization. From the square root of the induced heat one can see that the whole target area is not heated at once. By changing the phase as a function of time controller forms the optimal heat distribution in target area while minimizing the undesired heating in other subdomains.

6 Discussion

The controller iteration took typically 400-1000 iteration rounds. The line search might lower the computation time during the iteration. Another topic concerning the specification of the controller is to readjust weighting for the temperature distribution. As in all this type of control problems there are no general approaches to choose the weights. The weights for the temperature could, however, easily made adaptive (state dependent) so as to better approximate the physically more relevant inequality constraints for the temperature errors instead of the quadratic cost.

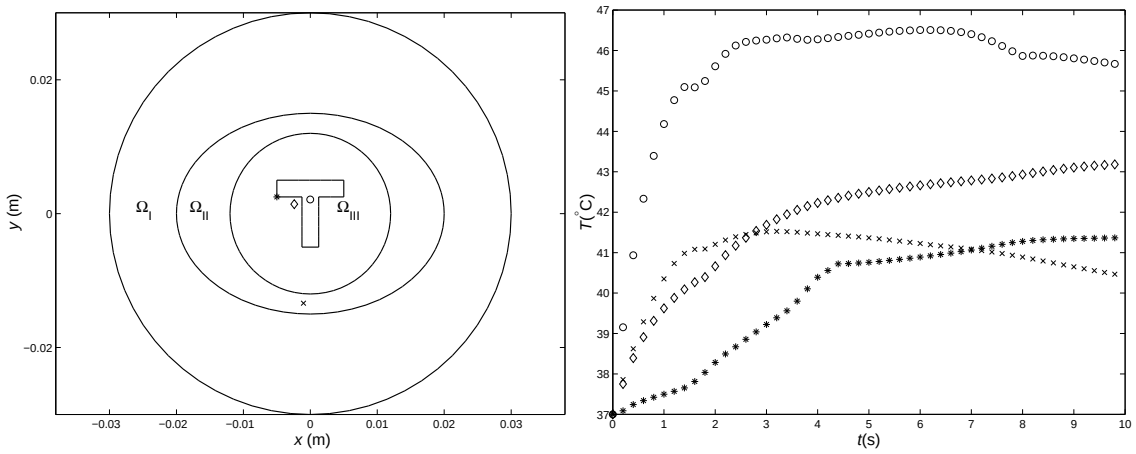

Figure 5: Left: the nodes in subdomains where the maximum temperatures was. There are also nodes for the maximum temperature (o) and the minimum temperature (*) for the target region. Right: The maximum temperatures in Ω_{II} (diamond), Ω_{III} (x) and the maximum (o) and the minimum (*) temperatures in the target

These adaptive weights are easy to include to the controller and they are usually obtained directly from the physical restrictions of the problem.

In many applications the material parameters are temperature dependent. These parameters can be easily taken into account with this control method. During the iteration, the FEM matrices are changed depending on the current temperature.

In the simulation example we used simple point sources for the ultrasound waves. More general transducer models are straightforward to implement in the UWVF and will affect only the fields.

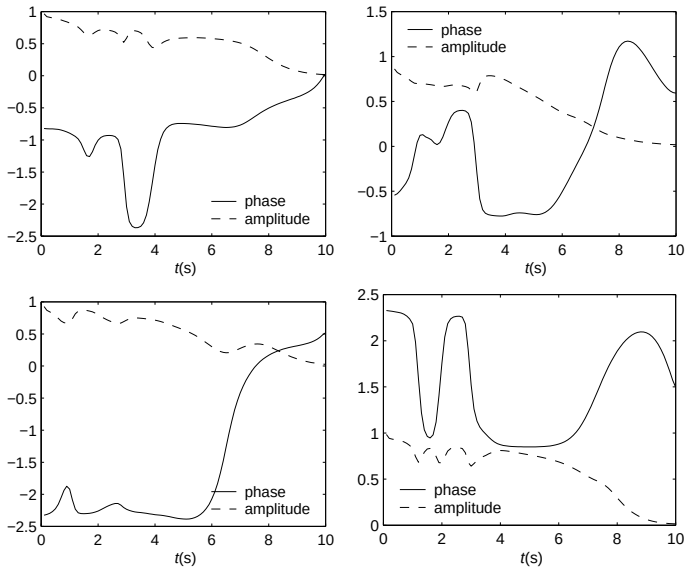

Figure 6: The phases and the amplitudes for point sources 6 (top left), 16 (top right), 26 (lower left) and 36 (lower right).

7 Conclusions

The controller which is proposed in this paper can be applied to ultrasound or microwave induced heating. In microwave induced heating the electrical field is computed from the Maxwell equations. The control algorithm is then applied to the problem in a similar way. The controller proposed here is an approximation for the optimal controller concerning quadratic costs with inequality constraints for the control variables. The simulation indicates that this method is able to produce accurate heat distributions in inhomogeneous media. The results from simulations was verified in different mesh to assess the robustness of the controller.

The simulation showed that this type of the controller can be applied also to hyperthermia treatment type problems. Another interesting applications might be sonochemical processing (Mason 2000). However, the main motivation of this paper

is the extension and modification of the proposed approach to ultrasound surgery (Duck *et al.* 1998), (Crum and Hynynen 1996). In ultrasound surgery the desired temperature is typically higher and the undesired heating must be minimized more accurately. In ultrasound surgery the main aim is to raise the thermal dose to the level that causes the necrosis of tissue (Daum and Hynynen 1999). The proposed controller can also be modified for thermal dose control. With direct control of thermal dose the peak temperatures can be decreased and the treatment time shortened (Daum and Hynynen 1999). The methods for thermal dose optimization in tissues include temporal switching (Daum and Hynynen 1999) and power adjusted focus scans (Wan *et al.* 1996).

When the proposed control method is used to thermal dose control the cost function is changed to weight the desired thermal dose distribution. The solution is found by similar gradient search. We have already implemented the modification for direct control of thermal dose (Malinen *et al.* 2003). The main advantage of using the proposed control method for thermal dose control is that the undesired thermal dose in healthy tissue can be directly minimized.

In most practical applications the control has to be done in three spatial dimensions, which makes the problem dimensions much larger and computing time consuming. On the other hand, the problem is physically and mathematically easier in 3D, which is the case for both boundary measurement and boundary control problems.

The advantage of using this type of a controller in the wave field induced heating problems is that this method does not need pre-focused wave fields. The main drawback of using the pre-focused ultrasound fields is that the ultrasound fields usually exhibit side lobes. These side lobes may cause undesired heating in the

healthy region. With the proposed control method the temperature distribution can be optimized in the target as well as in the healthy region. Yet another advantage is that the transducer limitations can be taken into account.

By introducing inequality constraints for state and control input the undesired heating in healthy tissue and maximum applied power for the transducers could be limited more accurately. Yet another further topic is to construct the feedback controller which uses the temperature measurements as a feedback to compensate the modeling errors in feedforward control. This can be done by linearizing the nonlinear state equation respect the feedforward trajectories for control input and temperature. Of course, the verification of the method in real 3D domains and with physical sonication. We are currently using a Linux cluster of 12 computers and parallelized implementation of the algorithms for the computation of UWVF and the controller in the corresponding 3D control problems with realistic geometries.

Acknowledgements

The project has been supported by the Finnish Academy grants 66592, 77818, 72431, 80773 and 200627.

A The Ultra weak variational formulation

A.1 The ultra weak variational formulation of the Helmholtz equation

Let us partition the domain of interest Ω with disjoint finite elements Ω_j and let ν_j denote the outward unit normal for j'th element. In addition, the boundary between

elements Ω_j and Ω_ℓ is denoted by $\Sigma_{j\ell}$. If the element Ω_j is on the boundary of the domain Ω, the coinciding boundary is denoted by $\partial\Omega_j \cap \partial\Omega = \Gamma_j$.

If the material parameters ρ and c are approximated with piecewise constant functions we can decompose the Helmholtz problem for all $1 \leq j \leq K$ as

$$\Delta p_j + \kappa_j^2 p_j = 0 \qquad \text{in } \Omega_j \tag{26}$$

$$\frac{1}{\rho_j}\frac{\partial p_j}{\partial \nu_j} - i\sigma p_j = -\frac{1}{\rho_\ell}\frac{\partial p_\ell}{\partial \nu_\ell} - i\sigma p_\ell \qquad \text{on } \Sigma_{j\ell} \text{ and for all } \ell \tag{27}$$

$$\left(\frac{1}{\rho_j}\frac{\partial p_j}{\partial \nu_j} - i\sigma p_j\right) = \tau\left(-\frac{1}{\rho_j}\frac{\partial p_j}{\partial \nu_j} - i\sigma p_j\right) + g \qquad \text{on } \Gamma_j \tag{28}$$

where $p_j = p|_{\Omega_j}$, $\tau \in \mathbb{C}$, $|\tau| \leq 1$, and the coupling parameter $\sigma > 0$, $\sigma \in \mathbb{R}$. The source term is denoted by g. The boundary condition for the problem can be adjusted with the parameter τ.

The boundary condition (27) is a coupled form of the transmission conditions which characterize the continuity of the pressure and the normal particle velocity across the interface $\Sigma_{j\ell}$ (Benamou and Despres 1997). The coupling parameter σ can be computed as the mean value of $\mathrm{Re}(\kappa)/c$ over the boundary

$$\sigma = \frac{1}{2}\left(\frac{\mathrm{Re}(\kappa_j)}{\rho_j} + \frac{\mathrm{Re}(\kappa_\ell)}{\rho_\ell}\right) \quad \text{on } \Sigma_{j\ell}. \tag{29}$$

We decompose the total wave p into two parts $p = p^{\mathrm{s}} + p^{\mathrm{inc}}$ where p^{s} is the scattered wave and p^{inc} is the incident wave. In this study the incident field is a point source of the form

$$p^{\mathrm{inc}} = \frac{i}{4}H_0^{(1)}(\kappa_j|r - r_0|)\,, \tag{30}$$

where r_0 is the location of the point source. The Sommerfeld boundary condition for the scattered part of the wave is obtained by choosing $\tau = 0$,

$$\sigma = \frac{\mathrm{Re}(\kappa_j)}{\rho_j}, \quad \text{and} \quad g = \left(\frac{1}{\rho_j}\frac{\partial p^{\mathrm{inc}}}{\partial \nu_j} - i\sigma p^{\mathrm{inc}}\right) \quad \text{on } \Gamma_j. \tag{31}$$

Define the function $f,\ f|_{\partial\Omega_j} = f_j$ on the element boundaries as follows

$$f_j = \left(\left(-\frac{1}{\rho_j}\frac{\partial}{\partial \nu_j} - i\sigma \right) p_j \right) \Bigg|_{\partial\Omega_j}, \quad 1 \le j \le K. \tag{32}$$

It is shown in (Cessenat 1996,C) that f_j satisfies *the ultra weak variational formulation, (UWVF)*

$$\begin{aligned} & \sum_{j=1}^{K} \int_{\partial\Omega_j} \frac{1}{\sigma} f_j \overline{\left(-\frac{1}{\rho_j}\frac{\partial}{\partial \nu_j} - i\sigma \right) q_j} \\ & - \sum_{j=1}^{K} \sum_{\ell=1}^{K} \int_{\Sigma_{j\ell}} \frac{1}{\sigma} f_\ell \overline{\left(\frac{1}{\rho_j}\frac{\partial}{\partial \nu_j} - i\sigma \right) q_j} \\ + & \sum_{j=1}^{K} \int_{\Gamma_j} \frac{t}{\sigma} f_k \overline{\left(\frac{1}{\rho_j}\frac{\partial}{\partial \nu_j} - i\sigma \right) q_j} \\ & = \sum_{j=1}^{K} \int_{\Gamma_j} \frac{1}{\sigma} g \overline{\left(\frac{1}{\rho_j}\frac{\partial}{\partial \nu_j} - i\sigma \right) q_j} \end{aligned} \tag{33}$$

for all test functions q_j which are the solutions of the adjoint Helmholtz equation

$$\Delta \overline{q}_j + \kappa_j^2 \overline{q}_j = 0 \quad \text{in } \Omega_j, \tag{34}$$

where the overbar denotes complex conjugation.

A.2 Discretization of UWVF

A Galerkin type approach can be applied to discretize the UWVF. In this approach the function (32) is approximated by a plane wave basis with compact support (Cessenat and Despres 1998)

$$f_j^a = \sum_{n=1}^{N_j} f_{jn} \left(-\frac{1}{\rho_j}\frac{\partial}{\partial \nu_j} - i\sigma \right) \varphi_{jn} \tag{35}$$

where

$$\varphi_{jn} = \begin{cases} \exp(i\overline{\kappa}_j d_{jn} \cdot r) & \text{in } \Omega_j \\ 0 & \text{elsewhere.} \end{cases} \tag{36}$$

For simplicity, a set of equally distributed plane waves d_{jn} is usually chosen

$$d_{jn} = \left(\cos\left(2\pi \frac{n-1}{N_j}\right), \sin\left(2\pi \frac{n-1}{N_j}\right) \right), \quad \text{for all } j \text{ and } n.$$

The functions φ_{jn} are also solutions of the adjoint Helmholtz problem and the Galerkin scheme is obtained by choosing $q_j \leftarrow \varphi_{jn},\ n = 1, \ldots, N_j$.

Substituting (35) and (36) to the equation (33) the problem can be written in the form of the matrix equation (Cessenat 1996), (Cessenat and Despres 1998)

$$(I - D^{-1}C)X = D^{-1}b. \tag{37}$$

where the unknowns $X = (f_{11}, \ldots, f_{1N_1}, \ldots, f_{KN_K})^T$ are to be determined. The matrices D and C are sparse and exhibit block structure. For example, D is a Hermitian block diagonal matrix consisting of the K blocks $D_k \in \mathbb{C}^{N_j \times N_j}$. To avoid the conditioning problems reported in (Cessenat and Despres 1998) we allow the number of bases N_j to vary between the elements as in (Huttunen *et al.* 2002).

¿From the equations (32) and (35) it follows that we can approximate the pressure field with

$$p^a = \sum_{n=1}^{N_j} f_{jn} q_{jn} \quad \text{on } \partial\Omega_j. \tag{38}$$

If $\kappa \in \mathbb{R}$ the equations (26) and (34) are equal and the approximation (38) is also valid within the element Ω_j. For $\kappa \notin \mathbb{R}$ – such as the case at hand – this is only an approximation. However, if the UWVF mesh and the heat equation meshes are appropriately adapted, we only need the UWVF solutions on the element boundaries.

B Heat source term in the FE bioheat equation

Since tissue boundaries are usually well defined, it is natural to consider meshes that are conformal with these boundaries, that is, the element boundaries coincide with the organ boundaries. In such a case it is also feasible to approximate $\alpha(r)$, $\rho(r)$ and $c(r)$ in the corresponding piecewise constant basis, that is, these material parameters are constants within each element. Furthermore, we approximate the $|p|^2$ distribution in the corresponding piecewise linear basis, that is, in the same basis as the temperature

$$|p|^2 = \sum_{p=1}^{N} \left| \sum_{k=1}^{m} \tilde{u}_k(t) \widetilde{C}_k(r_p) \right|^2 \varphi_p(r) \ . \tag{39}$$

Denote the FE source term vector by $Q_{\mathrm{D}}(t) \in \mathbb{R}^N$. We have for the j^{th} node

$$\begin{aligned} Q_{\mathrm{D},j}(t) &= \int_\Omega \frac{\alpha(r)}{\rho(r)c(r)} \sum_{p=1}^{N} \left| \sum_{k=1}^{m} \tilde{u}_k(t) \widetilde{C}_k(r_p) \right|^2 \varphi_p(r)\varphi_j(r)\, dr & (40) \\ &= \sum_{p=1}^{N} \left| \sum_{k=1}^{m} \tilde{u}_k(t) \widetilde{C}_k(r_p) \right|^2 \int_\Omega \frac{\alpha(r)}{\rho(r)c(r)} \varphi_p(r)\varphi_j(r)\, dr & (41) \end{aligned}$$

so that the associated modified mass matrix $\widetilde{M} \in \mathbb{R}^{N\times N}$ is specified by the elements

$$\widetilde{M}_{j,p} = \int_\Omega \frac{\alpha(r)}{\rho(r)c(r)} \varphi_p(r)\varphi_j(r)\, dr \ . \tag{42}$$

References

Babuska, I. and Melenk, J. M. 1997. The partition of unity method. *International Journal for Numerical Methods in Engineering*, **40**, 727–758.

Bardati, F., Borrani, A., Gerardino, A. and Lovisolo, G. A. 1995. Sar optimization in a phased array radiofrequency hyperthermia system. *IEEE Transactions on Biomedical Engineering*, **42**, 1201–1207.

Benamou, J. D. and Despres, B. 1997. A domain decomposition method for the Helmholtz equation and related optimal control problems. *Journal of Computational Physics*, **136**, 68–82.

Bhatia, A. B. 1967. *Ultrasonic Absorption: An Introduction to the Theory of Sound Absorption and Dispersion in Gases, Liquids and Solids.* (Dover Publications, Inc.).

Botros, Y. Y., Volakis, J. L., VanBaren, P. and Ebbini, E. S. 1997. A hybrid computational model for ultrasound phased-array heating in the presence of strongly scattering obstacles. *IEEE Transactions on Biomedical Engineering*, **44**, 1039–1050.

Botros, Y. Y., Ebbini, E. S. and Volakis, J. L. 1998. Two-step hybrid virtual array-ray (VAR) technique for focusing through the rib cage. *IEEE Transactions on Ultrasonics, Ferroelectrics, and Frequency Control*, **45**, 989–1000.

Burl, J. B. 1999. *Linear Optimal Control.* H_2 *and* H_∞ *methods.* (Addison-Wesley).

Cessenat, O. 1996. *Application d'une nouvelle formulation variationelle des equations d'ondes harmonigues, problemes de Helmholtz 2D et de Maxwell 3D.* Ph.D. thesis, Paris IX Dauphine.

Cessenat, O. and Despres, B. 1998. Application of an ultra weak variational formulation of elliptic PDEs to the two-dimensional Helmholtz problem. *SIAM Journal of Numerical Analysis*, **35**, 255–299.

Chapeleon, J. Y., Ribault, M., Birer, M., Vernier, F., Souchon, R., and Gelet, A. 1999. Treatment of localised prostate cancer with transresctal high intensity focused ultrasound. *European Journal of Ultrasound*, **9**, 31–38.

Chen, Y. Y., Lin, W. L., Liou, H. L., Yen, J. Y. and Shieh, M. J. 1999. Self-tuning fuzzy logic control for ultrasound hyperthermia with reference temperature based on objective functions. *Medical Physics*, **26**, 825–833.

Clement, G. T., Sun, J., Giesecke T. and Hynynen, K. 2000 A hemisphere array for non-invasive ultrasound brain therapy and surgery. *Physics in Medicine and Biology*, **45**, 3707–3719.

Crum, L. and Hynynen, K. 1996. Sound therapy. *Physics World*, 28–33.

Daum, D. R. and Hynynen, K. 1999. Thermal dose optimization via temporal switching in ultrasound surgery. *IEEE Transaction on Ultrasonics, Ferroelectrics and Frequency Control*, **45**, 208–215.

Daum, D. R. and Hynynen, K. 1999. A 256-element ultrasonic phased array system for the treatment of large volumes of deep seated tissue. *IEEE Transaction on Ultrasonics, Ferroelectrics and Frequency Control*, **46**, 1254–1268.

Diederich, C. J. and Hynynen, K. 1999. Ultrasound technology for hyperthermia. *Ultrasound in Medicine and Biology*, **25**, 871–887.

Doss, J. D. 1985. Simulation of automatic temperature control in tissue hyperthermia calculations. *Medical Physics*, **12**, 693–697.

Duck, F. A., Baker, A. C. and Starrit H. C. 1998 *Ultrasound in medicine* (Institute of Physics Publishing)

Ebbini, E. S. and Cain, C. A. 1989 Multiple-focus ultrasound phased-array pattern synthesis: optimal driving signal distributions for hyperthermia IEEE Transactions on Ultrasonics, Ferroelectrics and Frequency Control, **36**, 540–548.

Fan, X., and Hynynen, K. 1992. The effect of wave reflection and refraction at soft tissue interfaces during ultrasound hyperthermia treatments. *The Journal of the Acoustical Society of America*, **91**, 1727–1736.

Huttunen, T., Monk, P. and Kaipio, J. P. 2002. Computational aspects of the ultra weak variational formulation. *Journal of Computational Physics*, **182**, 27-46.

Hynynen, K. 1996. Focused ultrasound surgery guided by MRI. *Science & Medicine*, **3**, 62–71.

Ihlenburg, F. 1998. *Finite Element Analysis of Acoustic Scattering.* (Springer-Verlag).

Johnson, C. 1987. *Numerical Solution of the Partial Differential Equations by the Finite Element Method.* (Studentlitteratur).

Johnson, C., Kress, R, Roemer, R and Hynynen, K. 1990. Multi-point feedback control system for scanned, focused ultrasound hyperthermia. *Physics in Medicine and Biology*, **35**, 781–786.

Köhler, T., Maass, P. and Wust, P. 2000. Efficient Methods in Hyperthermia Treatment Planning. In Colton, D., Engl, H. W., Louis, A. K., McLaughling, J. R. and Rundell, W.(ed.) *Surveys on Solution Methods for Inverse Problems.* (Springer-Verlag), pp. 155-167.

Kowalski, M. E. and Jin, J. M. 2000. Determination of electromagnetic phased-array driving signals for hyperthermia based on a steady-state temperature criterion. *IEEE Transactions on Microwave Theory and Techniques*, **48**, 1864–1873.

Ku, H. S., Siu, F., Siores, E., Ball, J. A. R. and Blicblau, A. S. 2001. Applications

of fixed and variable frequency microwave (VFM) facilities in polymeric materials processing and joining. *Journal of Materials Processing Technology*, **113**, 184–188.

Kühnicke, E. 1996. Three-dimensional waves in layered media with nonparallel and curved interfaces: A theoretical approach. *The Journal of the Acoustical Society of America*, **100**, 709–716.

Lagendijk, J. J. W. 2000. Hyperthermia treatment planning. *Physics in Medicine and Biology*, **45**, R61–R76.

Lin, W-L., Roemer, R.B. and Hynynen, K. 1990. Theoretical and experimental evaluation of a temperature controller for scanned focused ultrasound hyperthermia. *Medical Physics*, **17**, 615–625.

Lin, W-L., Roemer, R. B., Moros, E. G. and Hynynen, K. 1992. Optimization of temperature distributions in scanned focused ultrasound hyperthermia. *International Journal of Hyperthermia*, **8**, 61–78.

Malinen, M., Huttunen, T. and Kaipio, J.P. 2003. Thermal dose optimization method for ultrasound surgery. *Physics in Medicine and Biology*, **48**, 745–762.

Mason, T. J. 2000. Large scale sonochemical prosessing: Aspiration and actuality. *Ultrasonics Sonochemistry*, **7**, 145–149.

Mattingly, M., Roemer, R. B. and Devasia, S. 2000. Exact temperature tracking for hyperthermia: A model-based approach. *IEEE Transactions on Control Systems Technology*, **8**, 979–992.

Monk, P. and Wang, D. 1999. A least squares method for the Helmholtz equation. *Computer Methods in Applied Mechanics and Engineering*, **175**, 121–136.

Morse, P. M. and Ingard, K. U. 1968. *Theoretical Acoustics.* (Princeton University Press).

Nikita, K. S., Maratos, N. G. and Uzunoglu, N. G. 1993. Optimal steady-state temperature distribution for a phased array hyperthermia system. *IEEE Transactions on Biomedical Engineering*, **40**, 1299–1306.

Pennes, H. H. 1948. Analysis of tissue and arterial blood temperatures in the resting human forearm. *Journal of Applied Physiology*, **1**, 93–122.

Pierce, A. D. 1991. *Acoustics: An Introduction to its Physical Principles and Applications.* (Acoustical Society of America).

Skinner, M. G., Iizuka, M. N., Kolios, M. C. and Sherar, M. D. 1998. A theoretical comparison of energy sources-microwave, ultrasound and laser-for interstitial thermal therapy. *Physics in Medicine and Biology*, **43**, 3535–3547.

Stengel, R. F. 1994. *Optimal Control and Estimation.* (Dover).

ter Haar, G. 1999. Therapeutic ultrasound. *European Journal of Ultrasound*, **9**, 3–9.

VanBaren, P. and Ebbini, E. S. 1995. Multi-point temperature control during hyperthermia treatments: Theory and simulation. *IEEE Transactions on Biomedical Engineering*, **42**, 818–827.

Visioli, A. G., Rivens, I. H., ter Haar, G. R., Horwich, A., Huddart, R.A., Moskovic, E., Padhani, A. and Glees, J. 1999. Preliminary results of a phase I dose escalation clinical trial using focused ultrasound in treatment of localised tumours. *European Journal of Ultrasound*, **9**, 11–18.

Wan, H., VanBaren P., Ebbini, E. S. and Cain, C. A. 1996. Ultrasound surgery: comparison of strategies using phased array systems. *IEEE Transactions on Ultrasonics, Ferroelectrics and Frequency Control*, **43**, 1085–1098.

Zohm, H., Kasper, E., Mehringer, P. and Müller, G.A. 2000. Thermal processing of silicon wafers with microwave co-heating. *Microelectronic Engineering*, **54**, 247–253.

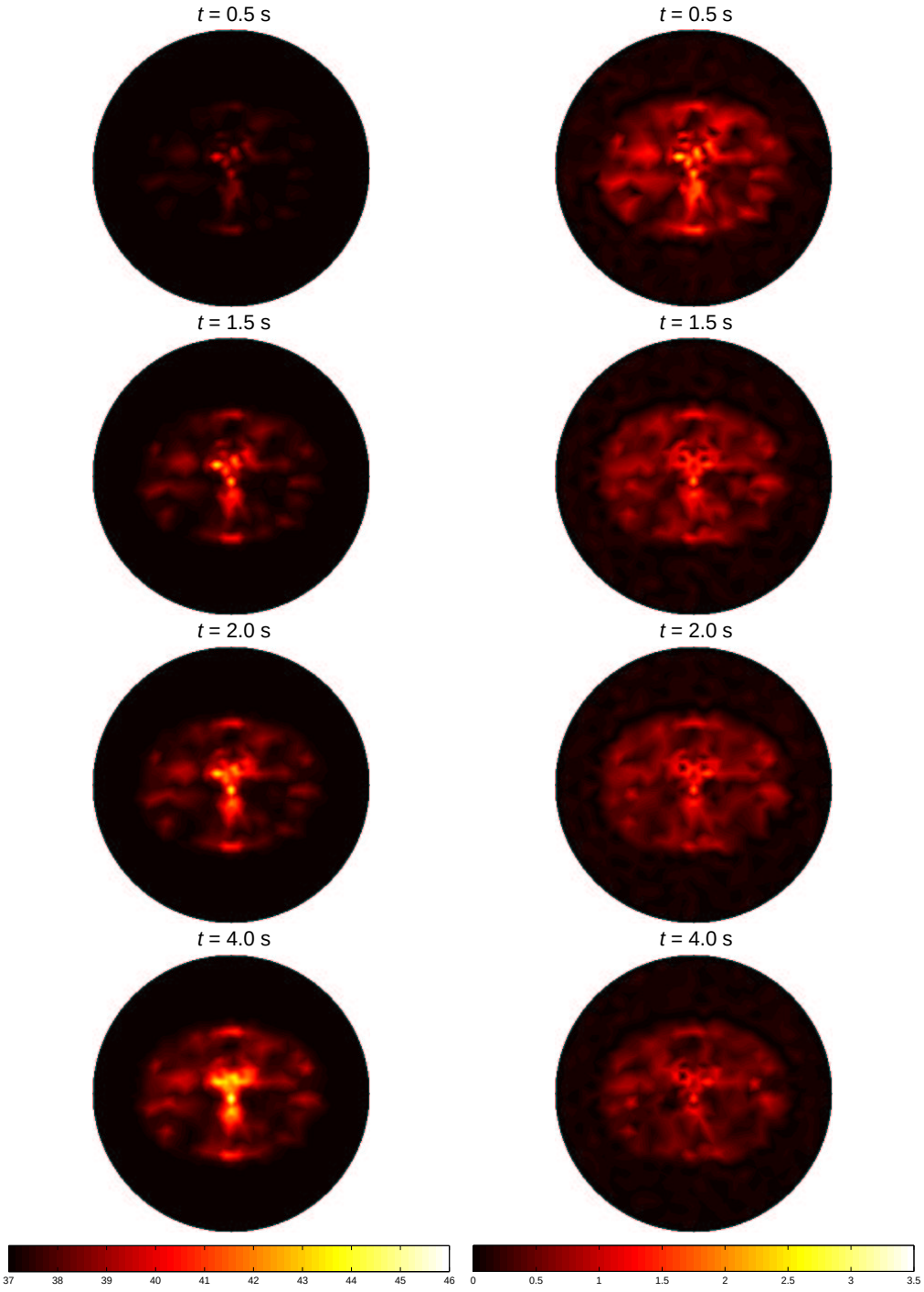

Figure 7: The temperature evolution in the sonication. The left hand row shows the temperature distribution and the right hand row shows the square root of the induced heat, that is, $\sqrt{M_{\mathrm{D}}(Bu)^2}$.

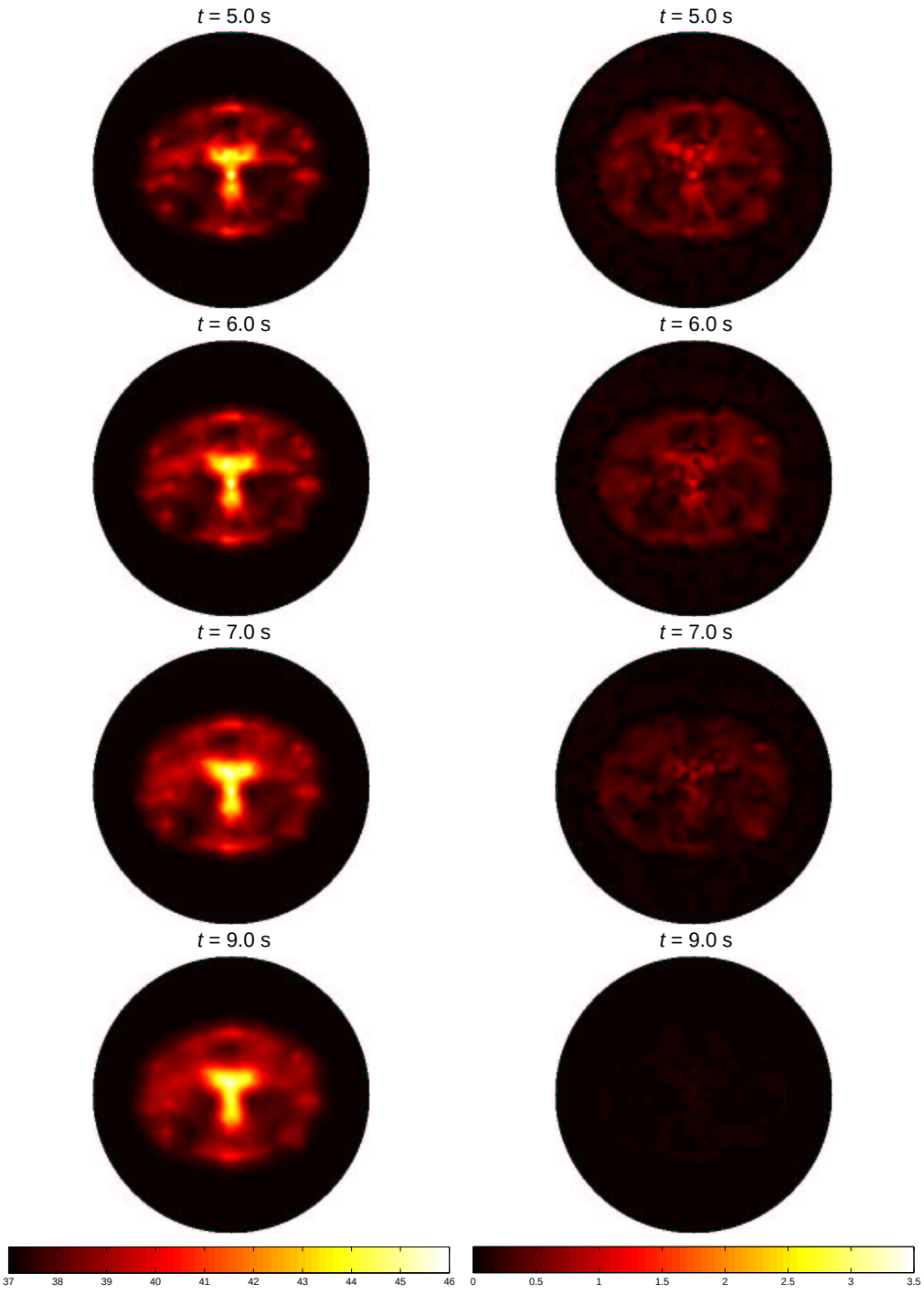

Figure 8: As in Figure 7